

19<sup>TH</sup> INTERNATIONAL SYMPOSIUM ON LASER-AIDED PLASMA DIAGNOSTICS  
22–26 SEPTEMBER, 2019  
WHITEFISH, MONTANA, U.S.A.

## Considerations for *in situ*, real time measurement of plasma-material interactions using Digital Holographic imaging

T.M. Biewer,<sup>a,1</sup> C.D. Smith,<sup>b</sup> T.E. Gebhart,<sup>a</sup> A. Greenhalgh,<sup>b</sup> X. Ren<sup>c</sup> and C.E. Thomas<sup>d</sup>

<sup>a</sup>Oak Ridge National Laboratory, Oak Ridge, TN 37831, U.S.A.

<sup>b</sup>University of Tennessee, Knoxville, TN 37996, U.S.A.

<sup>c</sup>Beloit College, Beloit, WI 53511, U.S.A.

<sup>d</sup>Third Dimension Technologies LLC., Knoxville, TN 37931, U.S.A.

E-mail: [biewertm@ornl.gov](mailto:biewertm@ornl.gov)

**ABSTRACT:** Digital Holographic (DH) imaging is a laser-based measurement technique, which can be used to monitor a material surface as it is being exposed to fusion-relevant plasmas. Both single-laser and dual-laser DH measurements have been demonstrated *ex situ* at Oak Ridge National Laboratory (ORNL). A DH diagnostic system is being assessed for deployment at ORNL to make *in situ*, real-time measurements of plasma erosion/redeposition in the Prototype Material Plasma Exposure eXperiment (Proto-MPEX). *In situ*, real time measurements pose unique challenges to diagnostic systems, which are not encountered by *ex situ* analysis techniques. The absolute surface height (tracked at the nm to  $\mu\text{m}$  position) during plasma exposure can be modified by: 1) surface movement due to vibration or thrust exerted by the plasma device, 2) surface growth due to the thermal expansion of the material under steady  $\text{MW/m}^2$  or transient  $\text{GW/m}^2$  plasma heat loads, and 3) surface modification due to plasma erosion/redeposition of the material substrate. To assess these effects, 1) the vibration spectrum of the diagnostic and the pulsed plasma device have been measured, 2) the thermal growth of the surface has been measured for an applied heat flux, and 3) the surface modification has been measured *ex situ* post plasma exposure, and *ex situ* post laser ablation as a proxy for the plasma. This paper will provide an overview of the results that have been achieved in the development of a DH diagnostic for *in situ* real-time measurements of plasma exposed surfaces in the Proto-MPEX device.

**KEYWORDS:** Plasma diagnostics - interferometry, spectroscopy and imaging; Overall mechanics design (support structures and materials, vibration analysis etc)

<sup>1</sup>Corresponding author.

---

## Contents

<b>1</b>	<b>Introduction</b>	<b>1</b>
<b>2</b>	<b>Vibration and motion considerations</b>	<b>2</b>
2.1	DH system vibration characterization	2
2.2	ET-Arc vibration characterization	4
2.3	Proto-MPEX vibration characterization	5
2.4	DH measurements of linear target displacement	5
<b>3</b>	<b>Thermal growth considerations</b>	<b>6</b>
<b>4</b>	<b>Erosion/redeposition considerations</b>	<b>9</b>
4.1	Proto-MPEX erosion observations	9
4.2	ET-Arc net erosion rates	10
4.3	Laser ablation as a proxy for plasma erosion	11
<b>5</b>	<b>Summary and future work</b>	<b>11</b>

---

## 1 Introduction

In the toroidal geometry of a magnetically confined fusion reactor, such as the International Tokamak Experimental Reactor (ITER), the high-temperature fusion plasma core is separated from the plasma facing components (PFCs) by a relatively lower-temperature boundary layer edge plasma. The transition from fusion core plasma to plasma edge occurs across a confinement “pedestal.” The particle and energy content of the edge plasma is largely determined by the performance of the confinement pedestal, but the edge plasma is also influenced by plasma-material interactions (PMI) occurring on the surface of the PFCs [1]. Heat and particles leave the ITER edge plasma primarily in the “divertor” region at the bottom of the device, where due to the magnetic geometry the boundary plasma is in contact with the material surfaces of the divertor plates at “strike points,” which are toroidal rings of intense PMI. Baseline H-mode operational scenarios of ITER are expected to deliver steady-state heat flux at the strike point of  $\sim 10 \text{ MW/m}^2$ . Intermittent relaxations of the confinement pedestal are ascribed to Edge Localized Modes (ELMs), during which the heat flux could transiently increase to  $> 10 \text{ GW/m}^2$ . Plasma-material interactions under these intense heat and particle loads will lead to material erosion, migration (potentially into the core plasma, degrading fusion performance), and redeposition.

PMI studies are an active area of research, directed toward engineering materials for PFCs which can survive in fusion reactor environments. Surface net erosion rates for a given material are typically determined *post mortem*, due to the fact that *in situ* surface measurement techniques are few or not available. The presence of high temperature plasma, the presence of magnetic

fields, and restricted access are all factors which constrain commonly available surface analysis techniques, such as scanning electron microscopes. Digital Holographic (DH) imaging is a laser-based measurement technique that is being developed at Oak Ridge National Laboratory (ORNL) to assess the effects *in situ* of fusion relevant plasma flux on material surfaces. Single-laser DH has been used “on the bench” at ORNL to measure *ex situ*  $\sim 100\text{ nm}$ – $4\text{ }\mu\text{m}$  surface features, and (differential) dual-laser DH has demonstrated measurements of  $\sim 5\text{ }\mu\text{m}$ – $2\text{ mm}$  surface features on static targets. This range of measurement is relevant to erosion effects anticipated for the ITER divertor plates during baseline ELM-ing operation, and for assessing erosion resulting from off-normal events, such as plasma disruptions and vertical displacement events (VDEs). A detailed description of the DH technique is given in previous publications [2–5]. This paper will describe the results of research in anticipation of deployment of the DH diagnostic for *in situ* measurements during plasma exposure of material surfaces.

DH will measure the surface height in an interrogation region ( $\sim 1\text{ cm}^2$ ) of a PFC during plasma exposure, ideally to ascertain the net erosion due to PMI. The surface height (as tracked *in situ* by the DH diagnostic at the nm to  $\mu\text{m}$  level) can be influenced by a variety of factors that arise during plasma exposure. These influences include: 1) vibration or solid-body motion of the surface relative to the DH diagnostic, 2) thermal growth of the surface due to high heat flux, and 3) net erosion/redeposition due to PMI. This paper will examine in section 2 considerations due to vibration and motion. Section 3 will discuss the expected thermal growth of the surface due to fusion relevant heat fluxes. Section 4 will outline *post mortem* erosion measurements from material targets exposed in plasma devices at ORNL to assess the relative magnitude of PMI erosion, in advance of *in situ* deployment of DH on these devices. Follow on work will be summarized in section 5, including conclusions.

## 2 Vibration and motion considerations

ORNL has several devices which can produce plasmas with a range of heat fluxes. The Prototype Material Plasma Exposure eXperiment (Proto-MPEX) has demonstrated plasma heat flux of  $\sim 5\text{ MW/m}^2$  onto material targets in pulsed operation [6]. Additionally, the ElectroThermal Arc (ET-Arc) source produces ELM-like transient plasma heat flux of  $1\text{--}2\text{ GW/m}^2$  [7]. These plasma sources have been used to prepare targets for *post mortem* DH measurements, and are being considered as test platforms for *in situ* DH measurements. This section will characterize the vibration level of the DH system in the context of minimum feature-height resolution. Measurements of the vibration spectrum and amplitudes for typical ET-Arc and Proto-MPEX discharges will be given. Lastly, “on the bench” DH measurements of programmed target movements will be shown, demonstrating the ability of the DH diagnostic to track the solid-body motion of dynamic surfaces.

### 2.1 DH system vibration characterization

The upper limit of the DH measurement range is nominally determined by the “ $2\pi$  phase ambiguity” that is inherent in the technique, which occurs when the surface feature height exceeds half the laser wavelength. The grating-tuned  $\text{CO}_2$  lasers used in the ORNL DH system have  $\lambda = 9.25\text{ }\mu\text{m}$  and  $\lambda = 9.27\text{ }\mu\text{m}$ . Hence, for single-laser DH operation the upper limit is  $\sim 9.26/2\text{ }\mu\text{m} = \sim 4.65\text{ }\mu\text{m}$ , and for the synthetic wavelength of dual-laser operation the limit is  $\sim 2\text{ mm}$ .

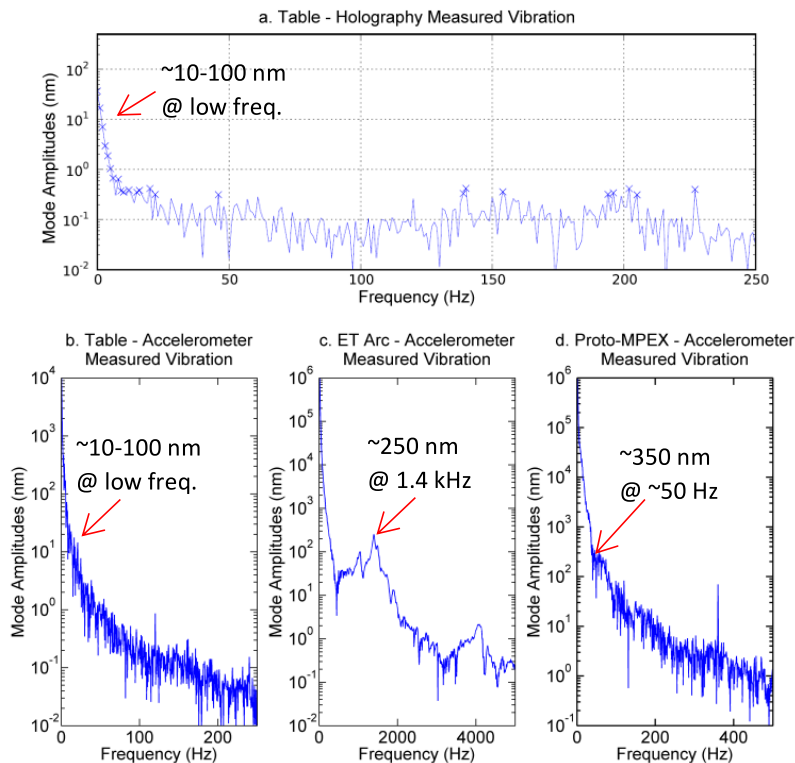


**Figure 1.** (a) Vibrational mode amplitudes measured using DH on the optical table, and accelerometer-measured amplitudes on (b) the DH optical table, (c) ET-Arc source, and (d) Proto-MPEX.

The lower limit of the DH measurement is a complicated convolution of the dynamic range of the camera, the dark noise of the camera sensor, the imaging optics, and the number of interference fringes used to construct the holographic image. This ideal limit is on the order of 10 nm for the ORNL single laser DH operation. However, for a given hardware configuration, the lower limit is functionally set by the vibration present in the system.

For *ex situ* measurements, where a *post mortem* target is placed on the DH laser table, the vibration-limit of the system can be measured using the DH system itself. Since the lasers are continuous wave (CW), the measurement frame rate is limited by the global full-frame read-out time. As with many digital camera arrays, this read-out time can be decreased by reducing the number of pixels in the digital array. For the ORNL system  $256 \times 256$  pixel typical frame rates are  $\sim 500$  Hz, while  $128 \times 128$  pixel frame rates can approach  $\sim 1500$  Hz. The recording duration of the ORNL DH system is limited to  $< 10$  s, which is set by the maximum time that the Stirling engine cooler (inside the FLIR SC4000 camera) can be suppressed. Mechanical vibration from the Stirling engine severely affects the interference fringe pattern when left running. When the Stirling engine is suppressed,  $\sim 10$  s is the approximate duration before thermal noise overwhelms the Quantum Well Infrared Photodetector (QWIP) array of the camera. These are important considerations to include when planning a future DH system upgrade with more modern equipment. Nevertheless, 10 s of data at 1 kHz frame rate implies that  $\sim 10,000$  images of a static target can be recorded. Since all the components are nominally stationary (except for vibrations), FFT analysis (shown in figure 1.a) of these 10,000 images allows for quantification of the vibration-limit of the system.

(Note: the CW laser light is acousto-optically modulated (AOM) with a usual setting of  $13\ \mu\text{s}$  “on” time, which is much less than the  $\sim 1\ \text{ms}$  camera framing period.) The envelope of surface height measurements suggests that the on-table DH lower resolution limit is  $\sim 100\ \text{nm}$  for single-laser operation and  $\sim 100\ \mu\text{m}$  for dual-laser operation; preliminary work has shown that the dual-laser lower limit can potentially be reduced to  $\sim 5\ \mu\text{m}$ .

An alternative method to measure the on-table DH vibration is through the use of an accelerometer. A triaxial 5-G accelerometer sensor (PCB Piezotronics sensor model 356B18) was placed at various locations on the DH table. The signals from this sensor were amplified by a PCB Piezotronics model 482C16 signal conditioner/amplifier, and displayed on a Tektronix model TDS 3014C oscilloscope with a Fourier analysis math function. In this way the dominant vibration frequencies and amplitudes (from the IR camera, the cooling water loops, chillers, laser power supplies, etc.) could be measured. An example spectrum is shown in figure 1.b. The accelerometer measurements suggest the dominant vibrations in the horizontal directions are on the order of tens of nm in the low frequencies, roughly consistent with the DH vibration-limit measurements on the laser path axis. The dominant vibration frequency in all cases is  $< 50\ \text{Hz}$ , possibly due to table modes or floor-induced vibrations.

## 2.2 ET-Arc vibration characterization

The accelerometer was also utilized to measure the vibration characteristics of the ET-Arc source during plasma discharges, since the ET-Arc is being assessed as a platform for *in situ* DH measurements. The ET-Arc parameters have been previously characterized [7]. The plasma discharge initiates in partial vacuum between a carefully designed cathode/anode pair, through a narrow channel in an ablative liner. The physical geometry of the ablative liner directs the high density ( $\sim 2.4 \times 10^{22}\ \text{electrons/m}^3$ ), low temperature ( $\sim 5\ \text{eV}$ ) plasma onto a nearby target plate for PMI studies. The fill gas in these experiments was He, the ablative liners were made of boron nitride (BN) ceramic, and the target plates were 6 mm thick 304 stainless steel. Previous measurements with an IR camera indicated that the heat flux on the target plate in these conditions is  $\sim 1\ \text{GW/m}^2$ , averaged over the 1 ms discharge. These parameters are similar to transient ELM heat fluxes and durations in high-performance tokamak plasma discharges [8].

The accelerometer head was placed on the outside of the vacuum chamber during a sequence of ET-Arc plasma discharges. During initial discharges the 5-G accelerometer sensor used for on-table DH measurements was found to be saturating, and was subsequently replaced with a 50-G sensor (PCB Piezotronics model 356A14). The oscilloscope was synchronized to the ET-Arc timing and accelerometer measurements indicate that there is a significant vibration in the vertical direction with an amplitude of  $\sim 250\ \text{nm}$ , and with a frequency of 1.4 kHz (see figure 1.c). Large low frequency amplitudes are also visible in figure 1.c; use of frame-to-frame holographic differential measurements during the plasma discharge, e.g. 500 Hz recordings, will allow the low frequency motion to be ignored. However, the 250 nm amplitude is still clearly much larger than the on-table DH vibrations. Hence, if the DH is staged for *in situ* measurements on the ET-Arc source, then the target motion relative to the DH table may limit the feature height resolution to  $> 250\ \text{nm}$  (if no mitigation is possible), assuming the target is secured to the vacuum vessel.

### 2.3 Proto-MPEX vibration characterization

Proto-MPEX utilizes an RF helicon antenna to produce high density, low temperature, light-ion (H, D, He) plasma in a cylindrical magnetic geometry, and is also being considered as a platform for *in situ* DH measurements [3, 6]. The magnetic field is established from  $t = 0$  to  $\sim 9$  s, with a “flat top” duration of constant field from  $t = 2$  to 6 s. In the middle of this steady field, the plasma discharge is initiated at  $t \approx 4$  s, for typical durations of 0.5 to 1.0 s. During this discharge duration, auxiliary electron and/or ion heating can be applied to the plasma column (with durations of 50 to 300 ms). The plasma column is directed onto a material target plate at the end of the device. Heat flux measurements on-target of  $\sim 5$  MW/m<sup>2</sup> have been reported [9], which is similar to the heat flux expected in ITER during baseline (inter-ELM) strike-point plasma exposure on the divertor plates.

A set of accelerometer measurements were made during Proto-MPEX plasma discharges. The currents in the magnet coils were  $\sim 3.5$  kA, resulting in peak B-field of  $\sim 0.5$  T near the target. Helicon-only discharges (no electron or ion auxiliary heating) of D<sub>2</sub> fueled plasmas with 60 kW of helicon forward power were studied, producing plasma on-target with electron density of  $\sim 1 \times 10^{19}$  m<sup>-3</sup> and temperature of 2 eV. During these operational conditions the 5-G accelerometer sensor was located on the exterior of the Proto-MPEX target chamber flange, and the oscilloscope was synchronized to the  $t = 4$  s plasma discharge initiation. Accelerometer measurements indicate that the dominant vibrations at  $\sim 50$  Hz are  $\sim 350$  nm in amplitude, with even higher amplitudes at low frequencies (see figure 1.d). The vertical direction is normal to the flange and perpendicular to the magnetic field and the plasma column. These amplitudes are larger than the on-table DH vibrations. Hence, if the DH is staged for *in situ* measurements on Proto-MPEX, then the target motion (if properly secured to the device) relative to the DH table will limit the feature height resolution (if no mitigation is achieved).

### 2.4 DH measurements of linear target displacement

A variety of target plates and mounts have been used in Proto-MPEX. Fast visible camera images of the target plate in certain mounts have shown significant displacement of the target surface. In particular, single-post mounted targets have shown deflections of several cm during high flux plasma impact. The plasma source concept of Proto-MPEX is similar to the VASIMR plasma thruster (using Ar gas) that is under development at NASA [10]. Hence it should not be surprising to observe such displacements for poorly secured targets. Properly secured targets have not shown such deflections within the resolution of fast visible camera measurements, and no attempt has been made to measure the plasma thrust in Proto-MPEX. However, an *in situ* real-time DH implementation that measures the surface height at the nm to  $\mu$ m level may nevertheless have to contend with residual surface displacement due to plasma thrust, depending on the target mount engineering.

To examine the limitations of such solid-body or piston-motion displacements on the *in situ* DH system capabilities, an *ex situ* experiment was performed. The on-table DH target was placed on a nano-positioning linear-drive stage (New Focus model 9063-B stage with model 8310 actuator), movable along the laser path axis. The motion of this stage could be programmed to execute fixed displacements of various distances. As described in section 2.1, the measurement window of the DH system is up to 10 s, during which period several displacements observable by the DH system are possible. Figure 2 shows the DH measured position of the average surface height as a function of

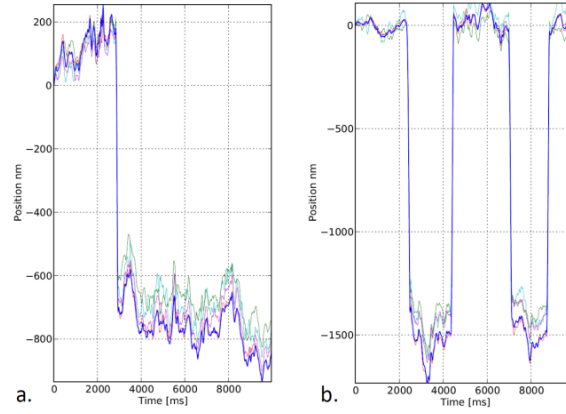


**Figure 2.** DH tracking of the average surface height during programmed motion of a target on a linear stage for a) single motion of 1  $\mu\text{m}$ , b) motion, return, motion, return of 1.5  $\mu\text{m}$ .

time. The DH system was able to track  $\mu\text{m}$  scale displacements without losing track of the surface. During the periods of no-motion, the pixel location fluctuates at the  $> 100$  nm level. This is a level of vibration that exceeds the previously measured on-table vibration-limit stated in section 2.1. However, it is likely that the mechanism of the nano-positioning stage is not as secure as a target firmly-mounted to the table. Hence it is reasonable that the stage-mounted targets exhibit a higher vibration-limit floor.

### 3 Thermal growth considerations

A macroscopic slab of material exposed to a heat flux,  $Q$ , at its surface will increase in temperature,  $\Delta T$ . This temperature increase will, in turn, lead to volumetric expansion of the material. Simple “back of the envelope” calculations can estimate the surface height change,  $\Delta h$ , due to this heat flux. Consider the slab of material shown in figure 3. Energy,  $E$ , incident on the surface will heat the material by an amount,  $\Delta T$ , according to the relation:  $E = C_{\text{SH}}m\Delta T$ , where  $m$  is the mass of the material, and  $C_{\text{SH}}$  is the specific heat capacity, which is material dependent. The mass of material is determined by the material density,  $\rho$ , through the relation  $\rho = m/V = m/(Ah)$ , where  $V$  is the volume of the slab found from the product of the area,  $A$ , and thickness,  $h$ . The energy incident on the surface is related to the heat flux through the relation  $Q = E/(A\Delta t)$ , where  $\Delta t$  is a period of unit time. These equations can be substituted to give:  $Q = E/(A\Delta t) = C_{\text{SH}}m\Delta T/(A\Delta t) = C_{\text{SH}}\rho Ah\Delta T/(A\Delta t)$ .

Eliminating the common surface area and solving for the temperature rise gives:  $\Delta T = Q\Delta t/(h\rho C_{\text{SH}})$ . The thermal growth of the slab in the laser path direction,  $\Delta h$ , is estimated using the relationship:  $\Delta h = C_{\text{TE}}h\Delta T$ , where  $C_{\text{TE}}$  is the coefficient of linear thermal expansion. By substituting the estimation of  $\Delta T$  derived above into this equation it is found that the original thickness of the material slab cancels out, resulting in the expression:

$$\Delta h = Q\Delta t C_{\text{TE}}/(\rho C_{\text{SH}}). \quad (3.1)$$

The accepted values for the material properties of several fusion-relevant materials are tabulated in table 1 for convenience. The last column of table 1 shows the capacity of these materials to

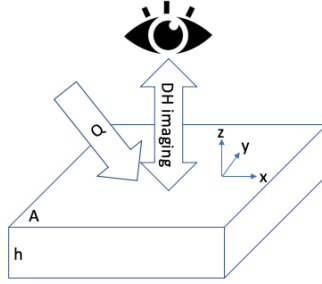


**Figure 3.** Heat flux,  $Q$ , incident on the surface (area,  $A$ ) of a slab of material (thickness,  $h$ ) with properties  $C_{SH}$ ,  $C_{TE}$ ,  $\rho$ , which is being observed by a Digital Holographic imaging system.

**Table 1.** Coefficients for fusion-relevant materials.

Material	$C_{TE}$ ( $10^{-6}/K$ )	$C_{SH}$ ( $J/g/K$ )	$\rho$ ( $g/cm^3$ )	$C_{TE}/\rho/C_{SH}$ ( $10^{-12} m^3/J$ )
St. Stl.	17.3	0.49	7.7	4.59
C (graph)	6	0.72	2.27	3.68
Be	12	1.82	1.85	3.56
W	4.5	0.13	19.3	1.79
SiC	4	0.75	3.1	1.72

manifest surface height growth for a given heat flux. This simple model only applies for heat loads which do not result in phase change (melting, sublimation) of the material of the slab; moreover, no consideration is given to heat conduction within the material or to heat dissipation from the supporting structure. As a plasma facing component, stainless steel will exhibit growth at a rate  $\sim 2.5\times$  that of tungsten, for example. Divertor tiles initially aligned or “fish scaled” to avoid leading-edges could potentially become misaligned at the  $\mu m$  level due to nonuniform incident heat fluxes. These misalignments could result in ever increasing nonuniformity of the heat flux due to the resultant thermal growth, in a runaway-like process.

Apart from these concerns, the DH diagnostic measurements are expected to track the surface height of plasma exposed targets at the nm to  $\mu m$  level (single-laser) and the  $\mu m$  to mm level (dual-laser). The intention is to demonstrate proof-of-principle *in situ* DH measurement on a plasma device at ORNL. Hence, it is important to estimate the thermal growth of the surface that could occur during these plasma exposures, so that the DH measurements of surface height are not misinterpreted as redeposition of material. Typical plasma heat flux and durations for the ET-Arc source are  $1 GW/m^2$  averaged over 1 ms. Proto-MPEX has achieved a variety of plasma discharge conditions, driven by a combination of the helicon plasma source power level and the inclusion of auxiliary electron and/or ion heating sources. The peak heat flux in Proto-MPEX has reached  $14 MW/m^2$  on target. The RF helicon source is nominally steady-state, however the ceramic window is not actively cooled, and the maximum duration plasma discharge has been administratively limited to  $< 2$  s. The most likely installation location for the DH diagnostic on Proto-MPEX is the “central chamber,” which precludes the use of the auxiliary electron and ion heating sources. Hence, the plasma heat flux available for DH measurements is likely to be  $< \sim 1 MW/m^2$ , with a duration  $\sim 1$  s.

**Table 2.** Surface height change due to the heat flux from three different sources, exhibiting their typical parameters, for some fusion-relevant materials.

	ET-Arc $Q = 1 \text{ GW/m}^2$ $\Delta t = 1 \text{ ms}$	Proto-MPEX $Q = 1 \text{ MW/m}^2$ $\Delta t = 1 \text{ s}$	Soldering Iron $P = 100 \text{ W}$ $A = 100 \text{ cm}^2$ $\Delta t = 100 \text{ s}$
Material	$\Delta h(\mu\text{m})$	$\Delta h(\mu\text{m})$	$\Delta h(\mu\text{m})$
St. Stl.	4.59	4.59	4.59
C (graph)	3.68	3.68	3.68
Be	3.56	3.56	3.56
W	1.79	1.79	1.79
SiC	1.72	1.72	1.72

Expected values of surface thermal growth that the DH diagnostic would encounter in these plasma devices for targets of various materials are shown in table 2. The parametric dependence of these estimates is easily extended using Equation 1, but in general the expected surface height growths are in the range measurable with the DH technique.

The accuracy of these estimates was tested “on the bench” by applying a soldering iron acting as a thermal point source to an otherwise static target, while observing the surface height with the DH system. The tip of the 100 W soldering iron was only  $\sim 1 \text{ mm}^2$ , however the applied heat was observed by an IR camera to spread laterally in the material slab/target; over the 10 to 100 s measurement duration the temperature of the entire  $10 \text{ cm} \times 10 \text{ cm}$  target plate was observed to rise. Hence, the area,  $A$ , used to estimate the heat flux in this student intern experiment was taken as the entire plate surface area. Figure 4 shows a plot of the DH measured surface height of a stainless steel target as a function of time for the soldering iron experiment. The soldering iron was applied for 10 s, and manifested  $\sim 400 \text{ nm}$  of surface growth. Figure 4 shows the period of cooling, after the soldering iron was removed. DH measurements during the heating phase of the experiment were complicated by conduction in the plate, and vibration/motion induced by the soldering iron. The DH measured average growth rate of the surface height  $\sim 400 \text{ nm}/10 \text{ s} = 40 \text{ nm/s}$  is in good

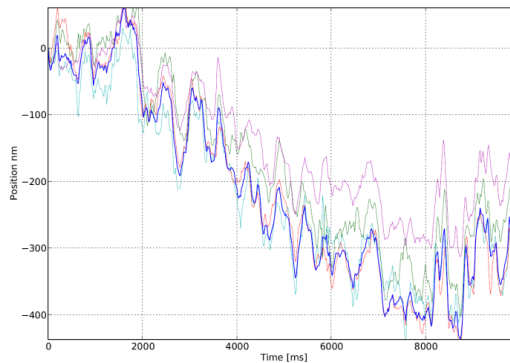


**Figure 4.** DH measured surface height vs. time as the surface temperature cooled, following 10 s application of the soldering iron to the target.

agreement with the prediction given in table 2 of  $4.59 \mu\text{m}/100 \text{ s} = 45.9 \text{ nm/s}$ . This gives confidence that the estimated thermal growth effects during plasma exposure heat loads will be of the order of magnitude predicted in table 2.

## 4 Erosion/redeposition considerations

The stated goal of the DH diagnostic is to measure net erosion rates from material surfaces due to plasma exposure, *in situ* and in real-time. This project is moving towards *in situ* proof-of-principle demonstration of the technique, and is assessing the viability of plasma sources at ORNL as justifiable test platforms for DH. *Post mortem* examination of targets exposed on Proto-MPEX and the ET-Arc source allow the net erosion rates to be assessed for suitability. These will be discussed in section 4.1 and 4.2, respectively. In advance of *in situ* deployment, a laser ablation system is available at ORNL and can be used as a proxy for plasma erosion, as will be discussed in section 4.3.

### 4.1 Proto-MPEX erosion observations

The mission of Proto-MPEX is to validate the plasma source concept for the planned Material Plasma Exposure eXperiment (MPEX). The milestone-driven research and development program of Proto-MPEX has been focused on retiring design risks for MPEX, and consequently the program has not devoted significant experimental time to investigating PMI effects. The Proto-MPEX target plate largely serves as a surface to terminate the plasma column on, as the plasma source and auxiliary heating physics are explored. Nevertheless, several target plates of differing materials have been utilized, including C (graphite), W coupons, SiC, and (usually) stainless steel.

Target plates, when removed from Proto-MPEX, have been examined *post mortem* by the DH system. Results previously reported have shown erosion features from 10 to  $40 \mu\text{m}$  in height on stainless steel targets during helicon-only operational periods of (non-continuous) weeks to months [11]. Other stainless steel targets have suffered sufficient heat flux to erode/melt through the thin plate in the presence of auxiliary heating. Re-crystallization of W on thin coupons has been observed [12]. Figure 5 shows a photograph of a SiC target, which exhibits a significant step from the masked to eroded region [13]. *Post mortem* DH measurements indicate this step is  $\sim 1.4 \mu\text{m}$  high,

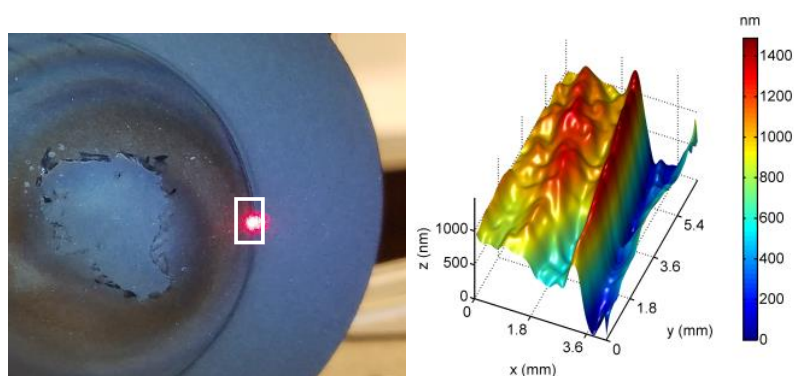


**Figure 5.** DH measurement (right) of a location (indicated by red laser dot inside white rectangle on photo, left) on the plasma-exposed SiC disc.

as shown in figure 5. This exposure was accumulated over several hundred 0.3 s plasma discharges during a 2 week period of operation. This suggests an average net erosion/redeposition rate of 10 to 50 nm/discharge, which will be challenging for DH to measure. Few of these experiments were conducted systematically to illuminate PMI effects. These examples qualitatively demonstrate and quantitatively suggest that Proto-MPEX can produce plasma discharges which will exhibit net erosion effects in the measurement range of DH imaging.

## 4.2 ET-Arc net erosion rates

The research demands on the ET-Arc source are significantly less than those of Proto-MPEX. Consequently, this research team was able to do a systematic evaluation of the net erosion rates achievable from ET-Arc plasma discharges. The ET-Arc discharges achieve high density via the incorporation of solid material from the ablative liner into the plasma. The plasma travels ballistically out of the liner channel and impacts the material surface with high heat and particle flux. The net change in surface height will be the balance between sputtered material leaving the target plate, and deposition of liner material onto the target plate. Unlike the procedure followed in previous work [7, 14], the residual material in these experiments is not removed in order to simulate the *in situ* measurement.

A target was fabricated that consists of two 304 stainless steel plates: a base plate and a cover plate. The base plate is the same geometry as a standard ET-Arc target plate, with some additional mounting holes conducive to repositionable *post mortem* DH analysis. The cover plate is removable, and secured to the base plate so as to cover half of the primary impact region of the plasma with the base plate. The top surface of each plate was polished to a  $\sim 600$  nm finish. The purpose of the cover plate is to shield a portion of the base plate from plasma exposure. An experimental cycle is followed: the target is exposed to ET-Arc plasma, removed for DH analysis (with cover plate on and off), and then returned for additional plasma exposure. In this way, the unexposed portion of the target base plate serves as a reference for subsequent DH analysis.

Single-laser DH images taken across the transition region from unexposed to exposed area show that there is a net removal of material from the base plate. Subsequent exposures, as shown in figure 6, imply that there is a net erosion of  $\sim 150$  nm of material for each ET-Arc plasma

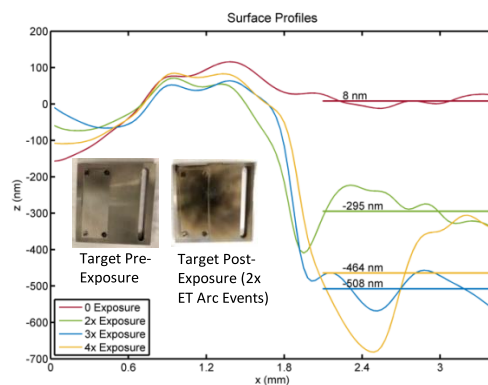


**Figure 6.** Single-laser DH measured profile of the net erosion from multiple ET-Arc plasma exposures. The unexposed region (shielded by the cover plate) is on the left, for  $x < \sim 1.8$  mm.

discharge. This finding indicates that the typical erosion produced by an ET-Arc plasma exposure can be expected to be within the DH measurable range, and therefore that the ET-Arc source may be coupled with the DH system for an *in situ* demonstration.

### 4.3 Laser ablation as a proxy for plasma erosion

As was discussed in section 3, the heat energy imparted to the material surface from plasma exposure results in thermal growth, which can complicate the use of DH *in situ* to measure net erosion over short duration recordings. An intermediate experiment could be to use a laser ablation system to create damage to the material surface (as a proxy to the plasma erosion) while minimizing thermal growth effects. The energy deposited at the surface ( $\sim 50$  to  $400$  mJ) by the laser is extremely focused, effectively vaporizing a local volume of the material to form an ablation crater, as shown in figure 7.

The diameter and depth of these craters is material and laser-energy dependent. By varying the laser energy from  $50$  to  $450$  mJ/pulse, the resultant crater depth can be varied between  $155$  to  $2200$  nm/pulse. The laser crater width as measured by single-laser DH, as shown in figure 7, is  $\sim 1.5$  mm. Hence, the laser ablation technique could be used as a proxy for plasma erosion to study dynamic erosion processes on-table with single-laser and differential dual-laser DH.

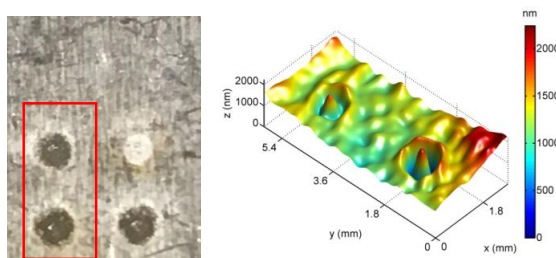


**Figure 7.** Single-laser DH image of laser ablation craters in a stainless steel target. Left: typical example of laser ablation pattern imaged by DH (see red rectangle). Right: DH image of a laser-ablated surface. The cone present in the crater is likely due to material which either was not removed by the laser pulse, or fell-back into the crater after ablation.

## 5 Summary and future work

Results from these single-effect experiments can be used to estimate the aggregate single-laser DH measurement, if implemented on Proto-MPEX and/or the ET-Arc source, as shown in table 3. Figure 8 presents the same data graphically for typical plasma discharges in Proto-MPEX and the ET-Arc Source. The three effects discussed in this paper are: 1) vibration/motion, 2) thermal growth, and 3) net erosion. For a dynamic, *in situ* DH measurement all three of these effects will be present (at differing levels) for the two platforms. In figure 8, the plasma discharge is initiated at  $t = 0$ . At that time, the vibration characterization changes from the on table “bench” measured amplitude and dominant frequency to those measured during the device pulsing. The thermal growth rate is initiated, as well as the erosion, at  $t = 0$ ; these persist until the end of the discharge, as is typical for each device. Post-discharge the thermal decay will depend on the mounting characteristics of the targets, but an exponential decay is assumed with a time constant of  $\sim 1$  s.

**Table 3.** Single-effect estimates of surface height displacement for various test conditions.

Surface height considerations	Vibration ( $\mu\text{m}$ )	Thermal ( $\mu\text{m}$ )	Erosion ( $\mu\text{m}$ )
DH “bench”	$\sim 0.100$ at $\sim 5$ Hz	–	–
Soldering Iron (100 W, 10 s)	–	0.400	–
Laser Ablation (per shot)	–	–	0.150 to 2.2
Proto-MPEX (per $1 \text{ MW/m}^2$ , 1 s shot)	$\sim 0.350$ At $\sim 50$ Hz	4.5	0.050
ET-Arc (per $1 \text{ GW/m}^2$ , 1 ms shot)	$\sim 0.300$ at 1400 Hz	4.5	0.150

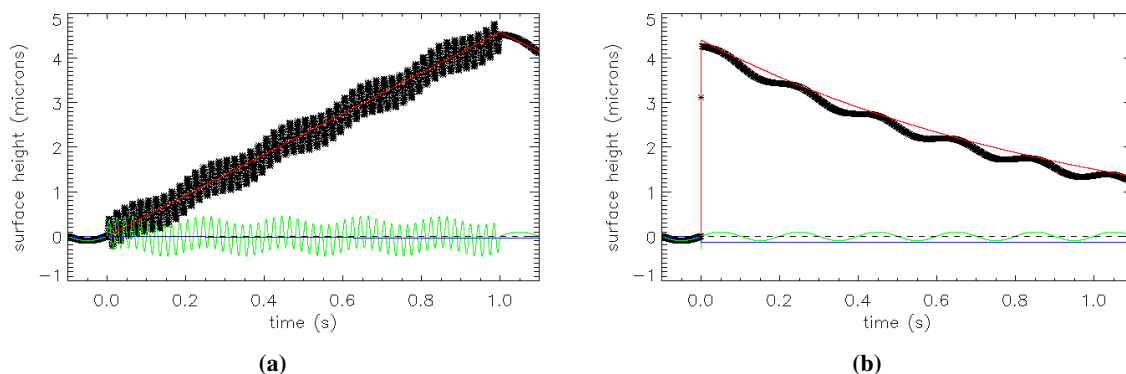


**Figure 8.** Surface height considerations for a stainless steel target (initial height, black dashed line) of vibration (green line) at dominant amplitude and frequency, thermal growth (red line), and erosion (blue line). The black \* are the sum of these three effects, displayed at the framing periodicity of the DH diagnostic. (a) Typical Proto-MPEX discharge of  $1 \text{ MW/m}^2$  for 1 s initiated at  $t = 0$ . (b) Typical ET-Arc discharge of  $1 \text{ GW/m}^2$  for 1 ms initiated at  $t = 0$ .

These results suggest that thermal growth effects due to the plasma heat flux will be the largest dynamic effect that the DH is likely to measure in either platform. The signature of the thermal growth would be distinctly different in the Proto-MPEX and ET-Arc cases, due to the different heat fluxes. This effect can be minimized by using target materials (e.g. SiC) that are less susceptible to thermal growth. However, the goal of the DH development is to demonstrate the measurement of PMI induced erosion. This will be challenging on both the Proto-MPEX “central chamber” and ET-ARC platforms. The single-shot erosion estimates are comparable to the inherent vibration-limit of the DH system, especially during the discharge(s). The short pulse of the ET-Arc system means that the period of vibrations is reduced, but also that the DH essentially measures at most 1 frame during the discharge. Nevertheless, it appears that the ET-Arc induced erosion is the best candidate for an *in situ* deployment of the DH system.

Future work will progress towards further improvements of the DH data processing technique, while the ET-Arc chamber is modified to allow for better access of the DH diagnostic. Since the on-table implementation of the laser ablation system is relatively straightforward, and thermal growth effects are minimized, an attempt will also be made to use the DH system to make dynamic measurements of laser ablations.

## Acknowledgments

This manuscript has been authored by UT-Battelle, LLC under Contract No. DE-AC05-00OR22725 with the U.S. Department of Energy. The United States Government retains and the publisher, by accepting the article for publication, acknowledges that the United States Government retains a non-exclusive, paid-up, irrevocable, world-wide license to publish or reproduce the published form of this manuscript, or allow others to do so, for United States Government purposes. The Department of Energy will provide public access to these results of federally sponsored research in accordance with the DOE Public Access Plan (<http://energy.gov/downloads/doe-public-access-plan>).

## References

- [1] G. Federici, P. Andrew, P. Barabaschi, J. Brooks, R. Doerner, A. Geier et al., *Key ITER plasma edge and plasma-material interaction issues*, *J. Nucl. Mater.* **313-316** (2003) 11.
- [2] C.E. Thomas, E.M. Granstedt, T.M. Biewer, L.R. Baylor, S.K. Combs, S.J. Meitner et al., *Digital holography for in situ real-time measurement of plasma-facing-component erosion*, *Rev. Sci. Instrum.* **85** (2014) 11D810.
- [3] C.E. Thomas, T.M. Biewer, L.R. Baylor, S.K. Combs, S.J. Meitner, J. Rapp et al., *Design of a digital holography system for PFC erosion measurements on proto-MPEX*, *Rev. Sci. Instrum.* **87** (2016) 11D624.
- [4] T.M. Biewer, J.C. Sawyer, C.D. Smith and C.E. Thomas, *Dual laser holography for in situ measurement of plasma facing component erosion (invited)*, *Rev. Sci. Instrum.* **89** (2018) 10J123.
- [5] C. Smith, T. Biewer, X. Ren, C. Thomas, T. Gebhart and Z. Zhang, *Recent Developments in Dual-laser Digital Holography for Plasma-Facing Surface Characterization*, *IEEE Trans. Plasma Sci.* (2019).
- [6] J. Rapp, T. Biewer, T. Bigelow, J. Caneses, J. Caughman, S. Diem et al., *Developing the science and technology for the material plasma exposure eXperiment*, *Nucl. Fusion* **57** (2017) 116001.
- [7] T.E. Gebhart, L.R. Baylor, J. Rapp and A.L. Winfrey, *Characterization of an electrothermal plasma source for fusion transient simulations*, *J. Appl. Phys.* **123** (2018) 033301.
- [8] A. Kreter, H.G. Esser, S. Brezinsek, J.P. Coad, A. Kirschner, W. Fundamenski et al., *Nonlinear impact of edge localized modes on carbon erosion in the divertor of the JET tokamak*, *Phys. Rev. Lett.* **102** (2009) 045007.
- [9] T.M. Biewer, C. Lau, T.S. Bigelow, J.F. Caneses, J.B.O. Caughman, R.H. Goulding et al., *Utilization of o-x-b mode conversion of 28 GHz microwaves to heat core electrons in the upgraded proto-MPEX*, *Phys. Plasmas* **26** (2019) 053508.
- [10] T.W. Glover, *Principal VASIMR results and present objectives*, in *AIP Conference Proceedings*, *AIP Conf. Proc.* **746** (2005) 976.

- [11] C. Smith, T. Biewer, C. Thomas, C. Beers and Z. Zhang, *Status of Dual-Laser Digital Holography for Surface Characterization at ORNL*, presented at *APS. Division of Plasma Physics Meeting*, Portland, OR, U.S.A., 5–9 November 2018, [CP11.076](#).
- [12] J.B.O. Caughman, R.H. Goulding, T.M. Biewer, T.S. Bigelow, I.H. Campbell, J. Caneses et al., *Plasma source development for fusion-relevant material testing*, *J. Vacuum Sci. Technol. A* **35** (2017) 03E114.
- [13] C. Beers, E. Lindquist, T. Biewer, J. Caneses, J. Caughman, R. Goulding et al., *Characterization of the helicon plasma flux to the target of proto-MPEX*, *Fusion Eng. Des.* **138** (2019) 282.
- [14] J.D. Coburn, T.E. Gebhart, C.M. Parish, E. Unterberg, J. Canik, M.W. Barsoum et al., *Surface erosion of plasma-facing materials using an electrothermal plasma source and ion beam micro-trenches*, *Fusion Sci. Technol.* **75** (2019) 621.